Pyrene Measurements in Sooting Low Pressure Methane Flames by Jet-Cooled Laser-Induced Fluorescence

ARTICLE *in* THE JOURNAL OF PHYSICAL CHEMISTRY A · DECEMBER 2011

Impact Factor: 2.69 · DOI: 10.1021/jp206970t · Source: PubMed

4 AUTHORS, INCLUDING:

Maxime Wartel
Université d'Orléans
25 PUBLICATIONS **59** CITATIONS
SEE PROFILE

Pascale Desgroux
Université des Sciences et Technologies de L…
93 PUBLICATIONS **1,149** CITATIONS
SEE PROFILE

Xavier Mercier
French National Centre for Scientific Research
39 PUBLICATIONS **471** CITATIONS
SEE PROFILE

THE JOURNAL OF PHYSICAL CHEMISTRY A

ARTICLE

pubs.acs.org/JPCA

Pyrene Measurements in Sooting Low Pressure Methane Flames by Jet-Cooled Laser-Induced Fluorescence

M. Wartel, J.-F. Pauwels, P. Desgroux, and X. Mercier*

Physico-Chimie des Processus de Combustion et de l'Atmosphère PC2A, UMR 8522 CNRS-Lille1 Plateforme de Métrologie Optique MeOL, Université Lille 1 Sciences et Technologies Cité scientifique, Bât C11/C5/CERLA, 59655 Villeneuve d'Ascq Cedex, France

ABSTRACT: This paper presents in detail the study we carried out concerning the pyrene measurement by jet-cooled laser-induced fluorescence (JCLIF) in different sooting low pressure methane flames. The aim of this paper is both to demonstrate the potentialities of this technique for the measurement of such moderately sized polycyclic aromatic hydrocarbons under sooting flame conditions and to provide new experimental data for the understanding and the development of chemical models of the soot formation processes. Several concentration profiles of pyrene measured in different sooting flame (various pressure and equivalence ratio) are presented. The validation of the JCLIF method for pyrene measurements is explained in detail as well as the calibration procedure, based on the standard addition method, which has been implemented for the quantification of the concentration profiles. Sensitivity lower than 1 ppb was obtained for the measurement of this species under sooting flame conditions.

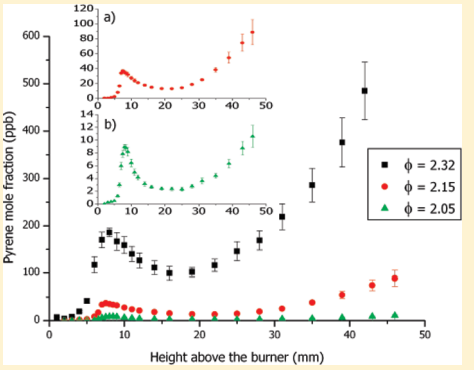

INTRODUCTION

The understanding of polycyclic aromatic hydrocarbons (PAH) and soot formation in combustion processes still remains a challenging task due to the involvement of complex physical and chemical mechanisms. The knowledge about the formation of PAH in flames has been considerably increased over the past few years because of the development of numerous and always more sophisticated experimental setups for their measurements[1−8] as well as the improvement of the modeling codes used to describe their formation.[9−11] Hence, the formation of soot particles has been demonstrated to be highly correlated to the production of PAH in flames by numerous studies. However large uncertainties remain concerning the chemical pathways and physical processes implicated in these mechanisms. From the experimental and modeling works of several groups[12−17] and the recent synthesis made by Wang[18] of these processes, the most probable pathways implicate the dimerization of PAH leading to stack clusters or cross-linked three-dimensional structures which are considered the elementary block of primary particles. Moreover, the close number of densities of moderately sized PAH and soot nuclei[18] would indicate that those PAH would be likely involved in the nucleation process of soot particles. From experimental works[19] and recent theoretical studies,[14,18] it has been established that the pyrene dimer could not survive at flame temperature (binding energy too low). However, pyrene is still considered in many models as the last gaseous PAH leading to soot nucleation. So, even if higher weighted PAH as coronene or circumcoronene should be more appropriate to initiate this nucleation step, the fact remains that pyrene is a key species in the mechanisms of soot formation. Experimental quantitative data relating to pyrene, as concentration profiles in laminar flames, are thus of great importance for the development and validation of those mechanisms.

Most of the experimental pyrene profiles reported in the literature have been determined by GCMS (gas chromatography mass spectroscopy).[2,5,20−28] Mass spectrometry is also used to measure this species in flames according to different setup configurations as MBMS (molecular beam mass spectrometry) with ionization by electron impact,[29] TOF/MS (time-of-flight mass spectrometry),[4,30] and more recently by coupling MBMS and a tunable synchrotron photoionization.[8]

In the present work, the measurement of quantitative profiles of pyrene has been carried out with an experimental setup similar to the one we have implemented for benzene and naphthalene measurements in several low pressure methane flames.[31,32] The use of methane flames, instead of the more sooting ethylene or acetylene flames, is motivated by the fact that the combustion of methane is representative of the combustion of the natural gas which is widely used in a lot of industrial burners. Moreover our laboratory has engaged a long-term work aiming to develop a kinetic model (GDF_kin)[33] specifically devoted to the understanding of methane combustion. Finally, another advantage of methane flames is linked to their low soot concentration compared to ethylene or acetylene flames, which reduces drastically the problem of clogging of the probe used for the sampling of species from flames.

This setup, which is only briefly described in this paper, is based on the extraction of the species from the flame by a thin microprobe and their drastic cooling inside an expanded free jet. Pyrene is then directly and selectively probed inside the expanded free jet by laser-induced fluorescence. Compared to the

Received: July 21, 2011
Revised: October 26, 2011
Published: October 27, 2011

Table 1. Experimental Flames Conditions[a]

	CH_4	O_2	N_2	pressure	eq ratio
flame 1	46.2%	39.8%	14%	200 Torr (26.65 kPa)	2.32
flame 2	44.6%	41.4%	14%	200 Torr (26.65 kPa)	2.15
flame 3	43%	42%	15%	200 Torr (26.65 kPa)	2.05
flame 4	46.2%	39.8%	14%	160 Torr (21.32 kPa)	2.32
flame 5	46.2%	39.8%	14%	140 Torr (18.66 kPa)	2.32

[a] Total flow rate = 3.96 l/min STP.

usual experimental techniques, this setup provides the advantages to be much less time expensive and enables real time measurements of pyrene concentrations in flames with a sensitivity estimated lower than 1 ppb.

As done for previous works, we present in a first part an experimental validation of the method for the measurement of pyrene. This analysis is based on the measurement of excitation and fluorescence spectra of pyrene as well as of its fluorescence lifetime under various experimental conditions.

The calibration procedure, which required the implementation of the so-called "standard addition method", is also explained in detail. Finally some concentrations profiles measured in different sooting flames are presented and discussed.

EXPERIMENTAL SETUP

The main part of the experimental setup is nearly the same as the one we used in previous studies for the measurement of benzene and naphthalene concentration profiles in different sooting and nonsooting flames. The main difference concerns the procedure of calibration.

The laser system consists of a Quantel Nd:YAG laser, pumping a dye laser (TDL70 Quantel). We used the second harmonic at 532 nm to pump the dye laser. DCM solved in ethanol was used for the oscillator and amplifier of the dye laser to generate by frequency doubling, a laser pulse around 321 nm. The beam was sent into the analysis chamber unfocused and spatially reduced (diameter approximately 2 mm) by a system of 2 lenses and 2 pinholes. The laser energy has been adjusted around 30 μJ/pulse to be in the linear regime of fluorescence. Fluorescence spectra were recorded via an Acton 2500i spectrometer (500 mm focal length—gratings with 1200 gr/mm or 300 gr/mm) which can be coupled either to a 16 bit intensified charge-coupled device camera (Roper Pimax II) or to a photomultiplier (Photonis XP2020Q, spectral range 150− 650 nm and maximum sensitivity around 420 nm). To increase the sensibility of the method, most of the concentration profiles have been determined by recording the pyrene fluorescence signals without the use of the spectrometer. In this case, a combination of three different filters (2 Schott long pass filters WG360, WG375 and a dielectric short pass filter with a 50% cutoff wavelength around 450 nm) have been used to define a spectral collection region comprised between 375 and 450 nm.

As in previous papers,[31,32] we choose to record the temporal integrated LIF signal rather than the peak intensity in order to optimize the signal-to-noise ratio.

The flat-flame burner (6 cm diameter) we used, provided by Holthuis & Associates, has also been described previously.[31,32] Measurements of pyrene have been carried out in different $CH_4/O_2/N_2$ flames stabilized for various conditions of pressure and equivalence ratio. In this paper are reported the experiments we made in 5 flames stabilized between 140 and 200 Torr (18.66 and

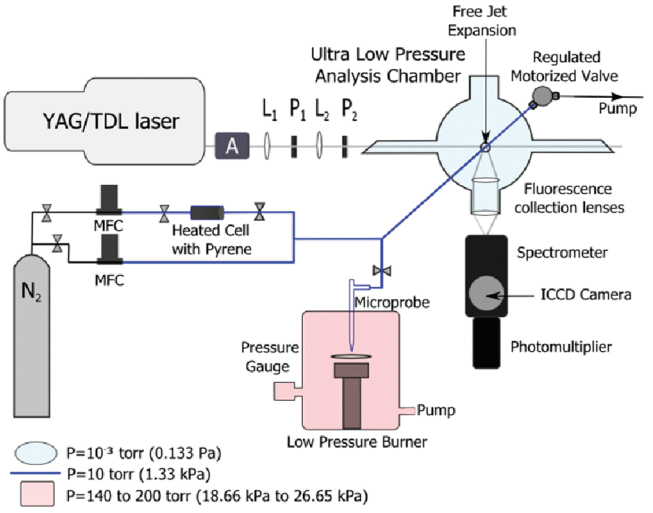

Figure 1. Experimental setup. A, variable attenuator; L_1 and L_2, converging lenses with 300 mm focal length; P_1 and P_2, pinhole with 2 mm aperture; MFC, mass flow controller.

26.65 kPa) for various equivalence ratios from 2.05 to 2.32. The flame conditions are reported in table 1. All these flames were considered as sooting flames featuring a yellow color characteristic of the soot particles. Note that we also tried to detect pyrene in nonsooting flames (Φ = 1.90) without success. The axially oriented microprobe for the sampling of the species was the same as the one previously used,[31,32] that is, a thin quartz tube (6 mm diameter) ended by a 20° conical aperture with a diameter of 300 μm. The Teflon line, represented in blue in figure 1, driving the species extracted from the flame to the analysis chamber was heated around 160 °C, while the pressure inside this line was maintained constant to 10 Torr (1.33 kPa) until the nozzle used for the free jet expansion. As discussed previously,[32] these sampling conditions (low pressure and heated line) ensure both the absence of condensation and limit the reactivity of the sampled species during their transport along the line. The pressure inside the analysis chamber was kept constant around 10^{-3} Torr (0.133 Pa). Species sampled from the flame are isentropically expanded into this analysis chamber through the nozzle aperture (1 mm orifice diameter) positioned at the center of this chamber. The laser axis was precisely adjusted inside the jet, 4 mm under the nozzle aperture, in order to make the LIF measurements of pyrene. Translating the burner vertically, concentration profiles of pyrene from 1 to 50 mm above the burner surface could have been recorded.

The calibration of the recorded LIF profiles has been done by the standard addition method. This method, which is detailed below, is based on the addition of small amounts of known and variable concentrations of pure pyrene to the species sampled from the flame. The device we used to generate these amounts of pyrene is reported in figure 1 and consists of a temperature controlled cell containing solid pyrene powder (Sigma Aldrich purity 98%). It is equipped with a porous filter (porosity of 0.5 μm) to prevent particles of solid pyrene to arrive in the analysis chamber. A controlled flow of N_2 is sent into this cell in order to generate a flow of pyrene vapor diluted in nitrogen. A second nitrogen flow is used to dilute this first flow of pyrene vapor allowing variable concentrations of pyrene to be produced. Both lines are heated around 160 °C, that is, the same temperature as the line providing the sampling of the species from the flame.

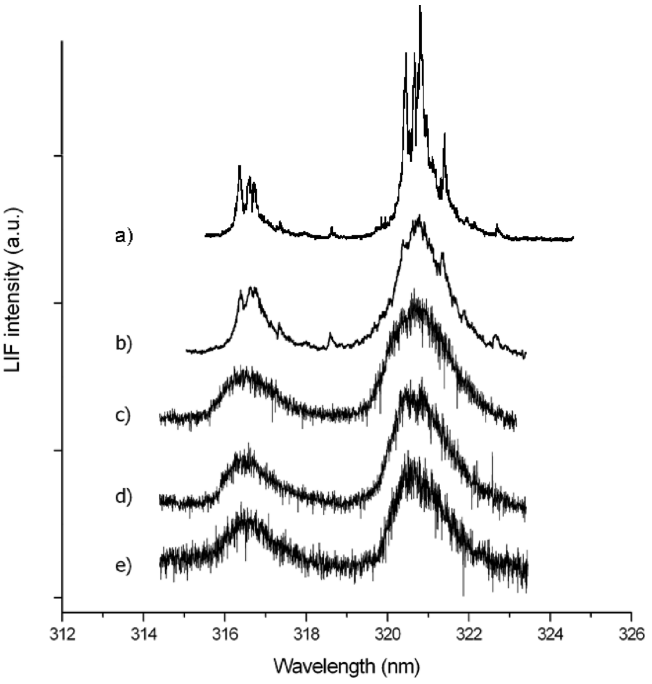

Figure 2. Excitation spectra of pyrene. (a) Pure pyrene diluted in argon, (Mangle et al.[39]). (b) Pure pyrene diluted in nitrogen (5 ppm, our work). (c) Pure pyrene diluted in nitrogen (300 ppb, our work). (d) Pyrene sampled from the flame (42 mm). (e) Pyrene sampled from the flame (8 mm).

As discussed below, it is very important that the nitrogen flow rate sent into the heated cell be slow enough to allow the saturation of this flow by the vapor of pyrene. This technique, known as the saturation gas phase method, is commonly used for measuring saturated vapor pressure of low volatile compound.[34] It involves the saturation of a carrier gas stream by the gas phase of a species in thermodynamic equilibrium with its solid phase. This aspect has been carefully taken into account in order to ensure that the vapor pressure of pyrene inside the line corresponds to its saturated vapor pressure under the temperature conditions of the cell. The value of the partial pressure of pyrene inside the cell has been determined by using the data issued from the work of Ruuzicka et al.[35] For all our experiments, the cell was thermostatted at a temperature of 50 °C, generating a saturated vapor pressure of pyrene of 9.67×10^{-5} Torr (1.29×10^{-2} Pa). The total pressure P_{total} inside the cell and along the line represented in blue in figure 1 was maintained constant and equal to 10 Torr (1.33 kPa).

Pyrene Spectroscopy. As for benzene and naphthalene, the oscillator strength of pyrene is stronger for transitions $S_2 \leftarrow S_0$ and $S_3 \leftarrow S_0$ than for the transition $S_1 \leftarrow S_0$. Yoshinaga et al.[36] determined the values of the first three transitions between singlet states equal to 1.4×10^{-3}, 3.3×10^{-1}, and 4.2×10^{-1}, respectively, for the S_1, S_2, and S_3 transitions. Another study carried out by Tanaka[37] led to barely similar experimental values, 1.6×10^{-3}, 3.3×10^{-1}, and 8.5×10^{-1} for the same transitions. The concentrations of pyrene being expected to be well below those of naphthalene, we have chosen the excitation of the $S_2 \leftarrow S_0$ band. This choice maximizes thus the sensitivity of the method but partly to the detriment of its spectral selectivity, the emission spectrum of fluorescence for a S_2 excitation leading indeed to a diffuse spectrum with less resolved structures compared to the fluorescence spectrum provided by a S_1 excitation. This point is clearly highlighted in the work of Borisevich et al.[38] where the structure of the fluorescence spectrum of pyrene after a $S_2 \leftarrow S_0$ excitation is shown to be wider and structureless than for a $S_1 \leftarrow S_0$ excitation. The reason of that loss of structure is mainly due to the large excess of energy involved for a S_2 excitation which implies a stronger contribution of nonradiative processes such as internal conversion (IC), intersystem crossing (ISC), and intravibrational redistribution (IVR). However it has been carefully determined that the spectral selectivity afforded by the S_2 transition was sufficient to detect selectively pyrene under sooting flames conditions.

Analysis of the Excitation and Emission Spectra. *Fluorescence Excitation Spectrum.* The approach to verify the selectivity of the experimental setup is based on the study of the excitation and fluorescence emission spectra. Figure 2 shows a comparison between the excitation spectrum (a) of pure pyrene diluted in argon, corresponding to the transition $S_2 \leftarrow S_0$ between 315 and 324 nm issued from the work of Mangle et al.[39] with the spectra we obtained according to various experimental conditions. The spectra (b) and (c) correspond respectively to the excitation spectra of pyrene diluted in nitrogen at 5 ppm and 300 ppb. Spectra (d) and (e) have been obtained from pyrene extracted from the reference flame ($\Phi = 2.32$ and $P = 200$ Torr (26.65 kPa)) for two different heights above the burner (h = 8 mm and 42 mm). The baselines of each spectrum have been vertically shifted for a better comparison.

We observe that the excitation spectrum of pure pyrene (Figure 2b) has a similar structure, in terms of position of the two vibrational bands, to the one obtained by Mangle et al.[39] It highlights an intense feature centered around 321 nm and a smallest one centered around 317 nm but appears clearly more congested and less spectrally resolved than the spectrum recorded by Mangle et al.[39] In addition, we also notice a slight difference in terms of intensity distribution of the vibrational bands of both spectra, reflecting a less effective cooling of the pyrene under our experimental conditions. As it is shown in the work of Rouillé et al.[40] where spectra of pyrene cooled down with argon and helium are reported, the gas carrier influences strongly the shape of the spectrum of pyrene. Moreover, the relative intensity of the two vibrational bands (317 and 321 nm) is very sensitive to the temperature as it has been observed in the work of Thöny et al.[41] for instance. Therefore concerning our experiments where pyrene is cooled down with a mixture of gases, the cooling is inevitably less efficient than it is by using Ar (Figure 2a) and some additional rotational structures or hot bands appear and degrade the global shape of the vibrational band (spectra b−e in Figure 2).

Furthermore, the spectra (Figure 2c) obtained from pure pyrene (300 ppb) and pyrene extracted from the flame (parts d and e of Figure 2) are too noisy to resolve the vibrational substructures. However, we observe that the overall structure of the spectrum is preserved in terms of position, bandwidth, and relative intensities between the two sets of vibrational bands whatever the gaseous environment of the pyrene, i.e., pure nitrogen or gases sampled from the flame. This comparison confirms that the spectrum of the pyrene issued from the flame is not affected by potential spectral interferences coming from other species, especially other PAH compounds, present in the flame. In the following of the paper, all the measurements have been performed by exciting the most intense vibrational band around 321 nm.

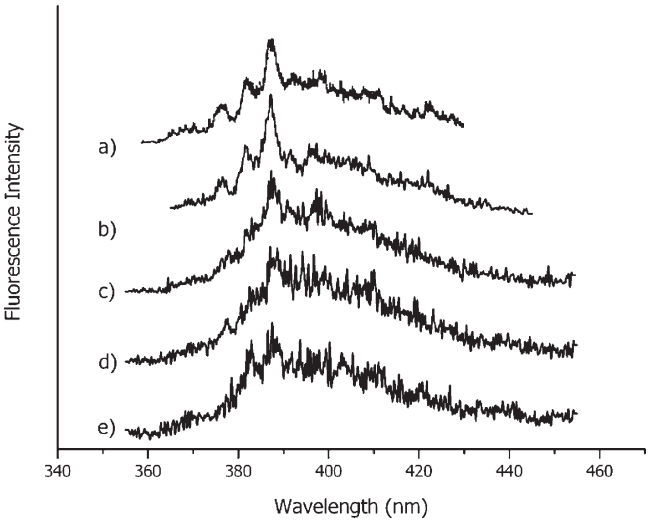

Figure 3. Fluorescence emission spectra of pyrene. (a) Pure pyrene diluted in argon (Numata et al.[42]). (b) Pure pyrene diluted in nitrogen (5 ppm, our work). (c) Pure pyrene diluted in nitrogen (1 ppm, our work). (d) Pyrene sampled from the flame (42 mm). (e) Pyrene sampled from the flame (8 mm).

Fluorescence Emission Spectrum. To confirm the selectivity of the method for the pyrene measurement in flames, we also checked the structure of the fluorescence emission spectra of pyrene for different conditions of gaseous environment. The fluorescence emission spectra obtained after the excitation of the origin of the transition $S_2 \leftarrow S_0$ around 321 nm are shown in Figure 3 in comparison with the one measured by Numata et al.[42] As expected, the excitation from S_0 to S_2 generates an emission fluorescence spectrum characterized by the presence of several vibronic bands with distinguishable broad band structures. These fluorescence emission spectra are found in good agreement with those issued from the literature,[38,42,43] whatever the concentration or the conditions of gaseous environment of the pyrene. As for the excitation spectra, we also note a slightly less structured and noisier shape, due to the less efficient cooling of our setup and above all the low concentrations of pyrene under flame conditions compared to the spectrum (Figure 3a) issued from the literature.[42] The comparison between the fluorescence emission spectrum of pure pyrene (parts b and c of Figure 3) with the spectra obtained from the pyrene issued from the flame (parts d and e of Figure 3) does not highlight spectral interferences, making significant intensity contributions by other species potentially fluorescent present in the flame unlikely. Moreover we did not notice as well any contribution of laser induced incandescence (broadband signal) potentially observable when sampling the pyrene in the sooting region of the flame (h > 10 mm). This last point confirms that the method is not affected by the presence of soot in the jet coming from the sampling gases of the flame.

Analysis of Fluorescence Lifetime. Another important point to check concerns the fluorescence lifetime of the pyrene, which is expected to be constant under the free jet conditions, whatever the sampling height above the burner. This assertion is indeed required for the determination of the concentration profile as well as for the validation of the calibration procedure.

Figure 4 presents a comparison of the fluorescence time decay determined from the pyrene extracted from the reference flame (h = 40 mm) with that obtained from pure pyrene diluted with

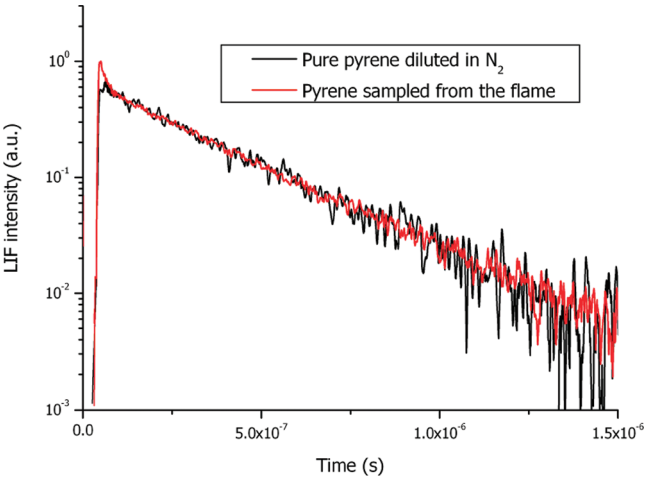

Figure 4. Fluorescence time decays of pure pyrene and pyrene sampled from the flame.

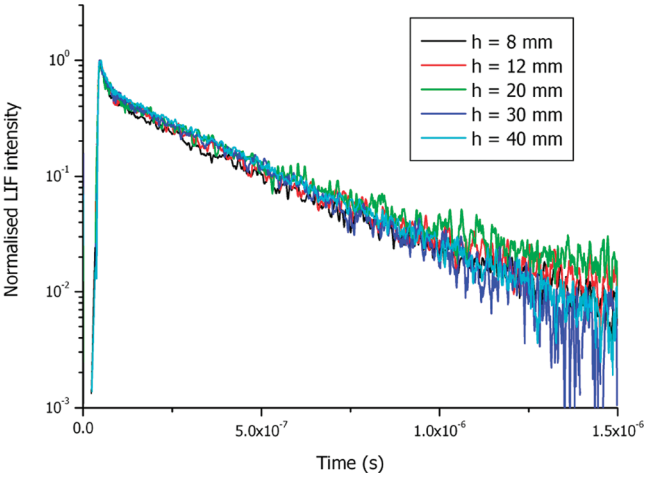

Figure 5. Fluorescence time decays of pyrene sampled from the flame for different heights above the burner.

nitrogen at the same concentration. As we can see from this figure, the measured fluorescence lifetime of pyrene highlights a slight different behavior during the first nanoseconds after the laser pulse according to the gaseous environment of the pyrene (pure N_2 or gases mixture sampled from the flame)

Therefore, although we did not previously notice any significant spectral differences according to the gaseous environment, we observe that the fluorescence lifetime of pyrene diluted in nitrogen is purely monoexponential (τ = 295 ns), while that of the pyrene extracted from the reference flame shows a biexponential feature with a long component (τ_1 = 294 ns) and a short one (τ_2 = 15 ns). We checked the absence of any scattering signal (wall, nozzle, ...) of the laser sent inside the analysis chamber which could have explained this behavior. Moreover, as it is presented in Figure 5, the short component of the fluorescence time decay appears when exciting pyrene sampling from the flame whatever the sampling height above the burner.

This slight different behavior of the fluorescence time decay can not be attributed to a spectral interference with another species sampled from the flame. We indeed did not observe any significant differences between the spectra of pure pyrene diluted

in nitrogen and pyrene sampled from the flame. Therefore, we believe that this phenomenon might be related to some different nonradiative processes promoted for the pyrene sampled from the flame. This biexponential behavior might indeed originate from a favorable coupling between the S_1 level and some of the near triplet states of the pyrene by intersystem crossing processes (ISC). It is to be noted that such biexponential fluorescence decays have already been mentioned in the literature, notably in the work of Werkhoven et al.[44] In this work, the authors also reported a short lifetime component of tens of nanoseconds during the excitation of the $S_1 \leftarrow S_0$, they attributed to a process of redistribution of energy of a specific vibration mode to some other vibration modes of the molecule (induced intravibrational redistribution process). Concerning our experiments, the presence or not of this short lifetime component is clearly correlated to the gaseous environment of the cooled pyrene. Therefore, it can be the result of a different cooling efficiency according to the carrier gas (nitrogen or species sampled from the flame) utilized for the free jet expansion. The other possibility is connected to the imperfect feature of the jet in terms of collisions at the point of measurement. Hence, if some very few collisions remain, it is likely that some species contained in the jet might induce such effects and slightly alter the fluorescence temporal decay.

The measurement of the fluorescence time decay has been done for different heights above the burner characterized by different gaseous environment. These measurements are reported in Figure 5. It appears that the biexponential behavior of the fluorescence signal does not evolve significantly. With concern for the decay time of the long component, it slightly increases by about 10% with the height of sampling from 8 to 40 mm. This slight variation is certainly due to the imperfect feature of free collision regime of the jet at the position of the laser measurement (i.e., 4 mm below the jet-generating nozzle). We indeed determined by calculation[45] that this position was located in the so-called "perturbed frozen region" of the jet by Mazely et al.[46] where some very few collisions can remain due to the sufficient density of the gases. We note that the variation of the long temporal component of the pyrene LIF signal is more significant for measurements done for the very first millimeters above the burner surface. This suggests so the presence of some potential quenchers of the pyrene fluorescence decreasing in concentration with the height above the burner. A likely collider as O_2, known as being a very efficient quencher of PAH,[47,48] and whose concentration decreases with the height above the burner, might be responsible for this phenomenon.

We already observed this effect in our previous work on naphthalene where a 2% variation of the temporal LIF signal had been observed. This study suggests so a greater dependence of the fluorescence process of pyrene to its gaseous environment during the cooling phase of the jet in comparison with smaller PAH. However this variation is still small, and the experimental uncertainty it induces is minored by the fact that we worked with the area of the temporal LIF signal. By this way, 10% uncertainties on the temporal decay only lead to 6% uncertainties on the corresponding area of the LIF signals. Therefore, the linear relationship between the time integrated signal and the pyrene concentration remains acceptable under our conditions.

For the determination of the concentration profiles, we choose the following protocol. In a first step, the relative concentration profiles corresponding to the measurements of the time integrated LIF signal according to the height above the burner are determined. Then, these relative concentration profiles are calibrated into absolute mole fraction profiles by the measurement of the pyrene mole fraction at the peak position of the profiles by using the standard addition method described below.

Calibration Procedure. In previous works done with this setup, the calibration of the LIF signal had been done thanks to a glass container filled with a known concentration of benzene or naphthalene diluted in nitrogen and directly connected to the analysis chamber. For the pyrene calibration, we did not use this method for two reasons. The first one is due to the differences observed between the temporal fluorescence decays of pure pyrene (monoexponential) and pyrene sampled from the flame (biexponential), which did not allow a direct comparison of the LIF signals. And the second one is related to the practical difficulties of filling a container with vapors of pyrene at a known concentration with a good accuracy given the very low vapor pressure of pyrene[35] (2.2×10^{-6} Torr at 20 °C) (2.93×10^{-4} Pa). To solve both of these difficulties, we implemented a calibration procedure based on the standard addition method.[49]

As previously said, the principle of this method relies on the addition of small amounts of known concentrations of pure pyrene to the flow of the pyrene sampled from the flame. The microprobe position being fixed in the flame, the concentration of the pyrene sampled from the flame is constant. By varying the concentration of the added pyrene to the pyrene sampled from the flame, the corresponding variation of the LIF signal measured in the jet is thus directly proportional to the concentration of the added pyrene. Doing this, we determine the calibration curve of the pyrene LIF signal. From this curve, we can show that the absolute value of the x intercept (LIF signal equal to zero) correspond the value of the concentration of the pyrene sampled from the flame at the height of sampling. This can be demonstrated as follows:

We ensured that the regime of fluorescence excitation was under the linear regime of energy, which allows in this case to consider the integrated LIF signal given by the following expression[48,50]

$$S_{\mathrm{LIF}} = \left(\frac{E}{h\nu}\right) V N_{\mathrm{py}} \phi(\nu, T) \sigma_{\mathrm{abs}}(\nu, T) \eta \frac{\Omega}{4\pi} \tag{1}$$

where $(E/h\nu)$ corresponds to the photons flux (in cm^{-2}), N_{py} the number density of pyrene in the observed volume V, η characterizes the collection efficiency of the optical setup, $\Omega/4\pi$ is the solid angle of collection, $\phi(\nu,T)$ the fluorescence quantum yield and $\sigma(\nu,T)$ the absorption cross section. We have shown previously that the temperature as well as the radiative and non radiative processes governing the fluorescence emission in the jet can be considered as constant whatever the sampling height above the burner. Therefore, by considering that LIF measurements were always done at the same position in the jet with the same laser wavelength and identical energy and that the emitted fluorescence photons were always collected coming from the same solid angle of collection and with the same efficiency, the expression (eq 1) simplifies and the fluorescence signal becomes only proportional to the molecular density of the pyrene excited inside the jet. It turns out that

$$S_{\mathrm{LIF}} = K N_{\mathrm{py}} = K X_{\mathrm{py}} \frac{N_a P_{\mathrm{total}}}{RT} \tag{2}$$

where X_{py} is the mole fraction of the pyrene, N_a the Avogadro number, R the gas constant, and T the temperature During the implementation of the standard addition method for the

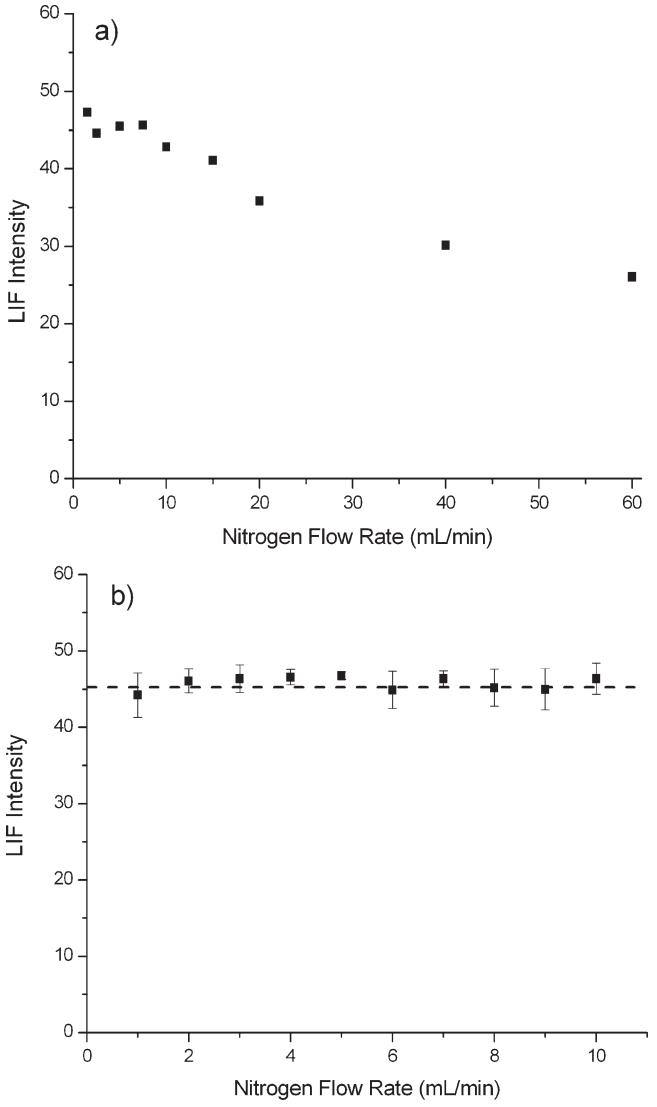

Figure 6. LIF intensity of the vapor phase of the pyrene issued from the cell carried by the nitrogen flow for different flow rates.

calibration, the measured fluorescence signal is thus proportional to the mole number of both added and sampled pyrene from the flame according to

$$S_{\mathrm{LIF}} = K\left[X_{\mathrm{py,\,flame}}\frac{N_a P_{\mathrm{total}}}{RT} + X_{\mathrm{py,\,added}}\frac{N_a P_{\mathrm{total}}}{RT}\right] \quad (3)$$

where $X_{\mathrm{py,added}}$ corresponds to the added mole fraction of pyrene. As the pressure and the temperature are constant parameters during all the experiments, the LIF signal at the measurement location in the jet can be expressed according to the mole fraction of the species to be measured $X_{\mathrm{py,flame}}$ and the known concentration species $X_{\mathrm{py,added}}$ as follows

$$S_{\mathrm{LIF}} = K'(X_{\mathrm{py,\,flame}} + X_{\mathrm{py,\,added}}) \quad (4)$$

where K' is thus a constant characteristic of the experimental conditions of the measurements.

The standard addition method requires the precise knowledge of the mole fraction of pyrene added to the pyrene sampled from the flame. To do this, we used a heated cell containing solid pyrene and electronically regulated in temperature (accuracy better than 0.1 °C). The flow rate of N_2 sent into the cell and acting as the carrier gas ($D_{\mathrm{carriergas}}$) has to be slow enough so that the vapor pressure of pyrene carried by the nitrogen flow does indeed correspond to the value of its saturated vapor pressure at the temperature of the cell.[34] The maximum flow rate of N_2, sent into the standard cell with solid pyrene which guarantees the saturation of the gas phase of the flow, has to be defined carefully. Parts a and b of Figure 6 show the evolution of the fluorescence signal of the pyrene measured for different flow rates of nitrogen. As expected, it appears that the measured fluorescence signal decreases when the nitrogen flow becomes greater than a certain value which was determined around 10 mL/min. This decrease in the signal intensity indicates indeed that the residence time of the nitrogen inside the cell is too short to enable its saturation by the pyrene vapors. A refining set of measurement on a shorter range of flow rates between 1 and 10 mL/min is also reported in Figure 6b. It shows that, within this flow range, the fluorescence signal remains constant whatever the nitrogen flow rate, reflecting the fact that the vapor pressure of pyrene carried by the nitrogen does indeed correspond to its saturated vapor pressure at the temperature of the experiment.

Under these conditions, the initial mole fraction of the added pyrene $X_{\mathrm{py,added,0}}$ is defined as the ratio of its partial pressure in the cell P_{py} to the total pressure inside the line

$$X_{\mathrm{py,\,added,\,0}} = \frac{P_{\mathrm{py,\,added}}}{P_{\mathrm{total}}} \quad (5)$$

The concentration of pyrene is modified through the dilution line (D_{dilution}) and the resulting flow is then added and mixed to the flow of pyrene sampling from the flame (D_{sampling}). We then varied the flow rates of the carrier gas to generate different concentrations while adjusting the flow rate of the dilution line in order that ($D_{\mathrm{carriergas}}$ + D_{dilution}) remain always constant and equal to 20 mL/min.

The pyrene mole fraction added to the sampling gases can therefore be written as

$$X_{\mathrm{py,\,added}} = X_{\mathrm{py,\,added,\,0}} \times \frac{D_{\mathrm{carriergas}}}{D_{\mathrm{carriergas}} + D_{\mathrm{dilution}} + D_{\mathrm{sampling}}} = X_{\mathrm{py,\,added,\,0}} \times \frac{D_{\mathrm{carriergas}}}{D_{\mathrm{total}}} \quad (6)$$

During all the experiments, the total pressure in the line was equal to 10 Torr (1.33 kPa) and the sampling flow rate determined around 80 mL/min. By varying the flow rate of the cell line from 1 to 9 mL/min, it allowed the addition of variable mole fraction of pyrene from 97 to 880 ppb without loosing the condition of full saturation of the carrier gas.

The mole fraction of the pyrene sampled from the flame $X_{\mathrm{py,flame,0}}$ is affected by the added flow of pure pyrene diluted in nitrogen and has to be scaled down by the corresponding factor of dilution

$$X_{\mathrm{py,\,flame}} = X_{\mathrm{py,\,flame,\,0}} \times \frac{D_{\mathrm{sampling}}}{D_{\mathrm{total}}} \quad (7)$$

From eqs 6 and eq 7 combined with eq 4, it follows that:

$$S_{\mathrm{LIF}} = K'\left[X_{\mathrm{py,\,added,\,0}} \times \frac{D_{\mathrm{carriergas}}}{D_{\mathrm{total}}}\right] + K'\left[X_{\mathrm{py,\,flame,\,0}} \times \frac{D_{\mathrm{sampling}}}{D_{\mathrm{total}}}\right] \quad (8)$$

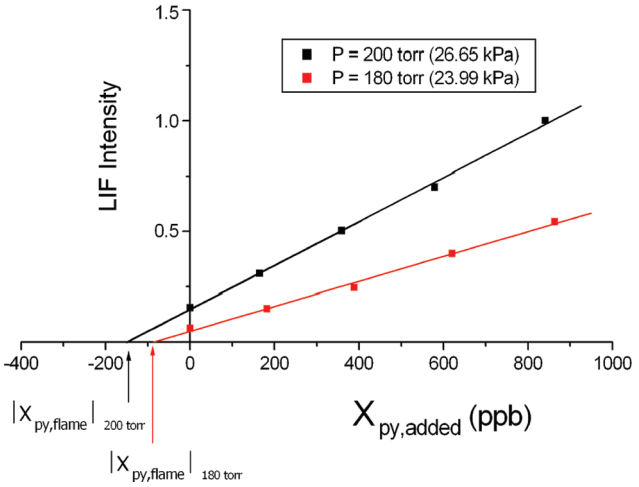

Figure 7. Calibration procedure using the standard addition method.

that is

$$S_{\mathrm{LIF}} = K' X_{\mathrm{py,\,added}}(\mathrm{variable}) + K' X_{\mathrm{py,\,flame}}(\mathrm{constant}) \quad (9)$$

therefore, it turns out that for $S_{\mathrm{LIF}} = 0$

$$X_{\mathrm{py,\,flame}} = |X_{\mathrm{py,\,added}}|_{S_{\mathrm{LIF}}=0} = X_{\mathrm{py,\,flame},0} \times \frac{D_{\mathrm{sampling}}}{D_{\mathrm{total}}} \quad (10)$$

Hence, the mole fraction of the pyrene sampled from the flame can be determined with the extrapolated value from the calibration curve $|X_{\mathrm{py,added}}|_{S_{\mathrm{LIF}=0}}$ according to the following expression

$$X_{\mathrm{py,\,flame},0} = |X_{\mathrm{py,\,added}}|_{S_{\mathrm{LIF}}=0} \times \frac{D_{\mathrm{total}}}{D_{\mathrm{sampling}}} \quad (11)$$

A valuable benefit of this method is that it allows a calibration of the LIF signal within the same gaseous environment than for the determination of the relative concentration profile of the pyrene from the flame.

As all additional gas flows required for the calibration method are accurately regulated, the main uncertainty concerning the concentration measurement with this method comes from the possible fluctuations of the flow rate of the gases sampled from the flame (that is the ratio $D_{\mathrm{total}}/D_{\mathrm{sampling}}$ in eq 11) partly because of the progressive clogging of the probe by the soot during the procedure. We thus determined the flow rate of the sampled gases for each point of the calibration curve. The observed variation of $D_{\mathrm{total}}/D_{\mathrm{sampling}}$, for the whole calibration curve, was in the worst case (for the more sooting flame) from the order of ±5% leading to uncertainties less than ±10% on the concentration measurements.

An example of the use of this method to calibrate the profiles of pyrene is reported in Figure 7 for two flames with the same equivalence ratio ($\phi = 2.32$) but different pressure ($P = 200$ Torr, 26.65 kPa) and ($P = 180$ Torr, 23.99 kPa). These measurements have been done for a sampling height of 8 mm above the burner (i.e., at the peak location of the pyrene profile).

The calibration curves appear, as expected, as straight lines whose intersections with the horizontal axis provide the value of the mole fractions of pyrene sampled from the flame. After correction due to the dilution caused by the additional flow of known concentrations of pyrene, we get the value of the mole fraction of the pyrene sampled 8 mm above the burner equal to 186 (±12) ppb for the 200 Torr (26.65 kPa) flame and 103 (±9) ppb for the 180 Torr (23.99 kPa) flame. This value which is 1.80 times lower than the value determined for the reference flame was in excellent agreement with the ratio of 1.84 of the LIF signal measured for this height (corresponding on the graph to the value of the LIF signal recorded for $X_{\mathrm{py,added}} = 0$). To limit the uncertainties of the calibration procedure, all the relative concentration profiles have been calibrated each other according to their LIF intensity and then quantified into absolute concentrations by using the mole fraction value obtained in the reference flame at 8 mm above the burner.

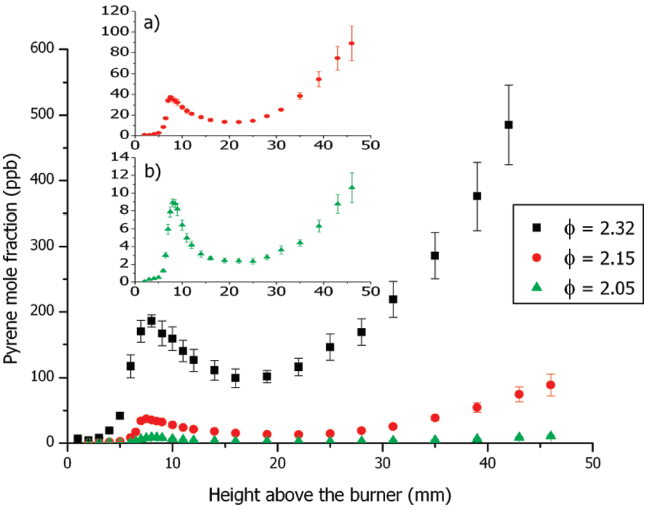

Figure 8. Mole fraction profiles of pyrene according to the height above the burner measured for different equivalent ratio at fixed pressure P = 200 Torr (26.65 kPa).

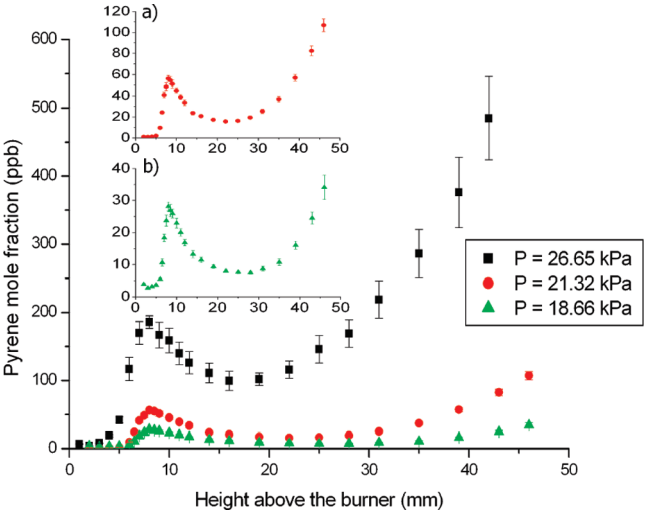

Figure 9. Mole fraction profiles of pyrene according to the height above the burner measured for different pressures at fixed equivalence ratio $\phi = 2.32$.

Experimental Profiles. The mole fraction profiles of pyrene have been measured for 5 different flames of $CH_4/O_2/N_2$ with various equivalence ratios and pressures (see table 1 for experimental conditions). The corresponding measured profiles are reported in Figures 8 and 9. All the reported profiles result from the average of at least two experimental profiles. The uncertainty bars shown on the graph represent an estimate of the experimental

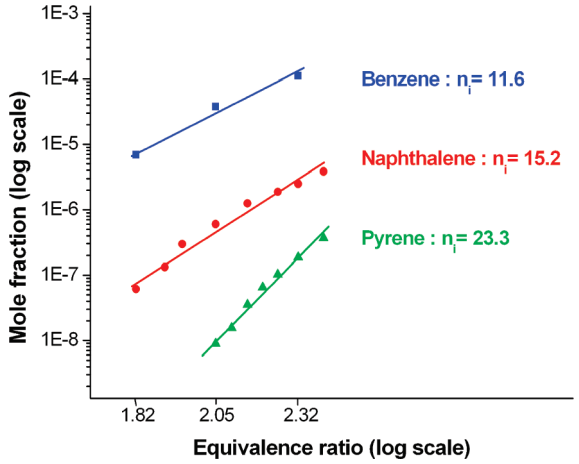

Figure 10. Logarithm of the first peak mole fraction of benzene, naphthalene, and pyrene according to the logarithm of the equivalence ratio at P = 200 Torr (26.65 kPa).

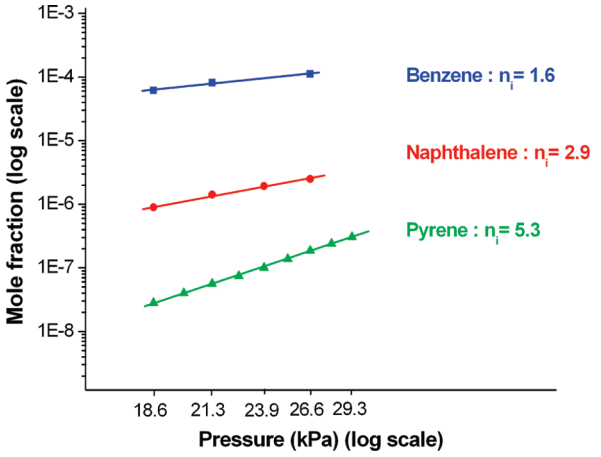

Figure 11. Logarithm of the first peak mole fraction of benzene, naphthalene, and pyrene according to the logarithm of the pressure at equivalence ratio Φ = 2.32.

uncertainties of our measurements, which takes into account the reproducibility of the LIF experiments as well as the uncertainties corresponding to the quantification phase done by the standard addition method. The limit of sensitivity of the method has been estimated to be lower than 1 ppb. This represents an improvement of a factor of 10 in comparison with the use of this setup for the measurements of naphthalene we studied previously.[32] This better sensitivity is explained by the use of a set of filters instead of a spectrometer for the measurements of the profiles and also by the higher oscillator strength of the $S_2 \leftarrow S_0$ transition of the pyrene comparatively to the $S_1 \leftarrow S_0$ transition used for the naphthalene measurements. It is interesting to note that no signal of pyrene could have been measured for flame equivalence ratio below ϕ = 2.05 which corresponds to the critical equivalence ratio for soot production under our flames conditions.

We observe that all the profiles highlight a similar shape as previously observed for benzene and naphthalene measurements. A first fast increase of the concentration until a maximum value followed by a decrease and a valley corresponding to an equilibrium between the chemical reactions of formation and consumption of pyrene. Finally, we note a strong reincrease of the concentration of the pyrene into the burnt gases, that is, in the sooting region of the flames whose onset appears around 10 mm above the burner in all flames.

As expected, the formation of the pyrene is promoted for higher pressures and equivalence ratios characterized by a strong increase of the concentration values measured at the first peak of the profiles. It is to be noted that the maximum of the peak of the profiles appears to be gradually less pronounced as the flames become more sooting. We observe that the beginning of decrease of pyrene concentration appears around 8−10 mm above the burner, i.e., just before the soot nucleation region which has been established around 10−12 mm for these flames.[51,52] This might denote a consumption of pyrene correlated to the formation of soot precursors. A modeling study has been engaged in order to explain the observed features.[53]

Another qualitative argument showing the importance of the pyrene in the soot mechanism can be characterized by plotting X_i (the mole fraction at the first peak of each profiles) according to the following power law[2,25,54] $A_i \times \phi^{n_i}$ (as we did previously for benzene and naphthalene[31,32]) where n_i defines the dependence of X_i to the equivalence ratio. A similar power law $A_i \times P^{n_i}$ can also be used to define the dependence of the formation of pyrene to the pressure. The exponent n_i was determined in previous works for benzene and naphthalene for equivalence ratio dependence. These data are reported here with the pyrene data in Figure 10. In addition, pressure dependence is shown for the 3 species in Figure 11. This representation, only gives a qualitative indication of the sensitivity of the formation of the species to pressure or equivalence ratio. Concerning the equivalence ratio study (Figure 10), it highlights for the pyrene a high value of the factor n_i equal to 23.3 in comparison with our previous works for which we found respectively a factor of 11.6 and 15.2 for the benzene and the naphthalene. For the pressure study (Figure 11), we found a factor of sensitivity equal to 5.3 within the range 140 to 220 Torr (18.66 to 29.32 kPa) while for benzene and naphthalene, we obtained, respectively, a factor of 1.6 and 2.9. We thus observe a clear trend showing a stronger pressure and equivalence ratio dependence of the PAH formation as their size increases. Concerning the pressure study, we determined elsewhere[51] that the soot mole fraction f_v was related to the pressure P according to the empirical law $f_v = KP^{n_i}$ with n_i =11. We can thus expect that the formation of higher weighted PAH such as coronene or ovalene might be characterized by n_i parameters closer to the one measured for the soot formation. This empirical factor could thus be an interesting parameter to characterized the last gaseous PAH to be taken into account in the models of soot formation.

CONCLUSION

Quantitative pyrene concentration profiles have been recorded using the jet-cooled LIF technique in 5 different sooting methane flames with various equivalence ratios and pressures. The potentiality of the method for the measurements of such PAH, in terms of selectivity and sensitivity, has been demonstrated. The detection limit of the jet cooled LIF method has been estimated lower than 1 ppb and did not seem to be affected by the presence of soot during the measurements. The measurements are well reproducible and obtained in real time, which enable fast acquisitions of pyrene mole fraction profiles. This method represents so an interesting alternative to usual methods for the selective measurements of such large PAH. Concerning

the measured concentration profiles of pyrene, it is interesting to note that they are well correlated with the previous benzene and naphthalene profiles we measured. A much more important dependence to the pressure and the equivalence ratio than previously reported for benzene and naphthalene has been highlighted. This last point reinforces the assumption of a stronger implication of the pyrene in the formation of soot precursors. Moreover, the fact that pyrene was not detectable with our setup in nonsooting flames ($\Phi < 2.05$), although benzene and naphthalene profiles have been previously measured in such flames (down to $\Phi = 1.82$),[31,32] could also indicate the importance of pyrene in the soot mechanisms processes even if a lack of sensitivity of the JCLIF method might also explain the absence of pyrene signal in nonsooting flame. We have recently measured the soot mole fraction profiles for all these sooting flames. The next step of this long-term project is the development of a kinetic model enabling to reproduce PAH and soot particles profiles. The first step has been reached for PAH[53] and will bring some chemical explanations about the formation of the pyrene and the importance of this molecule within the soot mechanism processes. Finally, we aim to extend the use of the JCLIF technique for the measurement of some higher weighted PAH such as coronene or ovalene in these same flames. Indeed, there are only very few measurements of these species reported in the literature while these species are expected to have a crucial importance in the soot formation processes.

AUTHOR INFORMATION

Corresponding Author

*Phone: +33 3 20 43 48 04. Fax: +33 3 20 43 69 77. E-mail: xavier.mercier@univ-lille1.fr.

ACKNOWLEDGMENT

The PC2A participates in the Institut de Recherche en ENvironnement Industriel (IRENI), which is financed by the Communauté Urbaine de Dunkerque, the Région Nord Pas-de-Calais, the Ministère de l'Enseignement Supérieur et de la Recherche, the CNRS, and European Regional Development Fund (ERDF). This work was also supported by the Agence Nationale de la Recherche (ANR-Contract 06-BLAN-0349).

REFERENCES

(1) Castaldi, M. J.; Marinov, N. M.; Melius, C. F.; Huang, J.; Senkan, S. M.; Pit, W. J.; Westbrook, C. K. *Proc. Comb. Inst.* **1996**, *26*, 693–702.
(2) Melton, T. R.; Inal, F.; Senkan, S. M. *Combust. Flame* **2000**, *121*, 671–678.
(3) Keller, A.; Kovacs, R.; Homann, K. H. *Phys. Chem. Chem. Phys.* **2000**, *2*, 1667–1675.
(4) Siegmann, K.; Sattler, K. *J. Chem. Phys.* **2000**, *112*, 698–709.
(5) Ciajolo, A.; Tregrossi, A.; Barbella, R.; Ragucci, R.; Apicella, B.; de Joannon, M. *Combust. Flame* **2001**, *125*, 1225–1229.
(6) Kamphus, M.; Braun-Unkhoff, M.; Kohse-Höinghaus, K. *Combust. Flame* **2008**, *152*, 28–59.
(7) Kitajima, A.; Hatanaka, T.; Takeuchi, M.; Torikai, H.; Miyadera, T. *Combust. Flame* **2005**, *142*, 72–88.
(8) Li, Y.; Tian, Z.; Zhang, L.; Yuan, T.; Zhang, K.; Yang, B.; Qi, F. *Proc. Comb. Inst.* **2009**, *32*, 647–655.
(9) Appel, J.; Bockhorn, H.; Frenklach, M. *Combust. Flame* **2000**, *121*, 122–136.
(10) Richter, H.; Granata, S.; Green, W. H.; Howard, J. B. *Proc. Comb. Inst.* **2005**, *30*, 1397–1405.
(11) Skjøth-Rasmussen, M. S.; Glarborg, P.; Østberg, M.; Johannessen, J. T.; Livbjerg, H.; Jensen, A. D.; Christensen, T. S. *Combust. Flame* **2004**, *136*, 91–128.
(12) Cain, J. P.; Camacho, J.; Phares, D. J.; Wang, H.; Laskin, A. *Proc. Comb. Inst.* **2011**, *33*, 533–540.
(13) Violi, A.; Kubota, A.; Truong, T. N.; Pitz, W. J.; Westbrook, C. K.; Sarofim, A. F. *Proc. Comb. Inst.* **2002**, *29*, 2343–2349.
(14) Herdman, J. D.; Miller, J. H. *J. Chem. Phys. A* **2008**, *112*, 6249–6256.
(15) Miller, J. H. *Proc. Comb. Inst.* **1991**, *23*, 91–98.
(16) Happold, J.; Grotheer, H.-H.; Aigner, M. *Combustion Generated Fine Carbonaceous Particles*; Bockhorn, H., D'Anna, A., Sarofim, A. F., Wang, H., Eds.; KIT Scientific Publishing: Karlsruhe, 2009; pp 275−288.
(17) D'Anna, A. *Combustion Generated Fine Carbonaceous Particles*; Bockhorn, H., D'Anna, A., Sarofim, A. F., Wang, H., Eds.; KIT Scientific Publishing: Karlsruhe, 2009; 287−320.
(18) Wang, H. *Proc. Comb. Inst.* **2011**, *33*, 41–67.
(19) Sabbah, H.; Biennier, L.; Klippenstein, S. J.; Sims, I. R.; Rowe, B. R. *J. Phys. Chem. Lett.* **2010**, *1*, 2962–2967.
(20) Bockhorn, H.; Fetting, F.; Wenz, H. W. *Ber. Bunsen−Ges. Phys. Chem.* **1983**, *87*, 1067–1073.
(21) Ciajolo, A.; D'Anna, A.; Barbella, R.; Tregrossi, A. *Proc. Comb. Inst.* **1994**, *25*, 679–685.
(22) Castaldi, M. J.; Senkan, S. M. *Combust. Sci. Technol.* **1996**, *116*, 167–181.
(23) Huang, J.; Senkan, S. M. *Proc. Comb. Inst.* **1996**, *26*, 1631–1637.
(24) Senkan, S.; Castaldi, M. *Combust. Flame* **1996**, *107*, 141–150.
(25) Melton, T. R.; Vincitore, A. M.; Senkan, S. M. *Proc. Comb. Inst.* **1998**, *27*, 1631–1637.
(26) Ergut, A.; Granata, S.; Jordan, J.; Carlson, J.; Howard, J. B.; Richter, H.; Levendis, Y. A. *Combust. Flame* **2006**, *144*, 757–772.
(27) D'Alessio, A.; D'Anna, A.; D'Orsi, A.; Minutolo, P.; Barbella, R.; Ciajolo, A. *Proc. Comb. Inst.* **1992**, *24*, 973–980.
(28) Marinov, N. M.; Pitz, W. J.; Westbrook, C. K.; Vincitore, A. M.; Castaldi, M. J.; Senkan, S. M.; Melius, C. F. *Combust. Flame* **1998**, *114*, 192–213.
(29) Bittner, J. D.; Howard, J. B. *Proc. Comb. Inst.* **1981**, *18*, 1105–1116.
(30) Hepp, H.; Siegmann, K.; Sattler, K. *Chem. Phys. Lett.* **1995**, *233*, 16–22.
(31) Mercier, X.; Wartel, M.; Pauwels, J. F.; Desgroux, P. *Appl. Phys. B: Lasers Opt.* **2008**, *91*, 387–395.
(32) Wartel, M.; Pauwels, J. F.; Desgroux, P.; Mercier, X. *Appl. Phys. B: Lasers Opt.* **2010**, *100*, 933–943.
(33) El Bakali, A.; Dagaut, P.; Pillier, L.; Desgroux, P.; Pauwels, J. F.; Rida, A.; Meunier, P. *Combust. Flame* **2004**, *137*, 109–128.
(34) Wania, F.; Shiu, W.-Y.; Mackay, D. *J. Chem. Eng. Data* **1994**, *39*, 572–577.
(35) Ruuzicka, K.; Mokbel, I.; Majer, V.; Ruuzicka, V.; Jose, J.; Zábranský, M. *Fluid Phase Equilib.* **1998**, *148*, 107–137.
(36) Yoshinaga, T.; Hiratsuka, H.; Tanizaki, Y. *Bull. Chem. Soc. Jpn.* **1977**, *50*, 2548–2553.
(37) Tanaka, J. *Bull. Chem. Soc. Jpn.* **1965**, *38*, 86–102.
(38) Borisevich, N. A.; Vodovatov, L. B.; Dyachenko, G. G.; Petukhov, V. A.; Semenov, M. A. *Laser Phys.* **1997**, *7*, 400–402.
(39) Mangle, E. A.; Topp, M. R. *J. Phys. Chem.* **1986**, *90*, 802–807.
(40) Rouillé, G.; Krasnokutski, S.; Huisken, F.; Henning, T.; Sukhorukov, O.; Staicu, A. *J. Chem. Phys.* **2004**, *120*, 6028–6034.
(41) Thöny, A.; Rossi, M. J. *J. Photochem. Photobiol., A* **1997**, *104*, 25–33.
(42) Numata, Y.; Nirasawa, T.; Suzuka, I. *J. Photochem. Photobiol., A* **2010**, *209*, 27–31.
(43) Hermine, P. PhD thesis, Université de Paris XI Orsay, 1994.
(44) Werkhoven, C. J.; Deinum, T.; Langelaar, J.; Rettschnick, R. P. H.; van Voorst, J. D. W. *Chem. Phys. Lett.* **1975**, *30*, 504–509.
(45) Wartel, M. Doctoral thesis, University of Lille1, 2011.
(46) Mazely, T. L.; Smith, M. A. *J. Chem. Phys.* **1988**, *89*, 2048–2062.

(47) Koban, W.; Koch, J. D.; Hanson, R. K.; Schulz, C. *Appl. Phys. B: Lasers Opt.* **2005**, *80*, 777–784.
(48) Orain, M.; Baranger, P.; Rossow, B.; Grisch, F. *Appl. Phys. B: Lasers Opt.* **2010**, *100*, 945–952.
(49) Gittins, C. M.; Castaldi, M. J.; Senkan, S. M.; Rohlfing, E. A. *Anal. Chem.* **1997**, *69*, 286–293.
(50) Koban, W. Doctoral thesis, Ruperto-Carola University, 2005.
(51) Desgroux, P.; Mercier, X.; Lefort, B.; Lemaire, R.; Therssen, E.; Pauwels, J. F. *Combust. Flame* **2008**, *155*, 289–301.
(52) Faccinetto, A.; Desgroux, P.; Ziskind, M.; Therssen, E.; Focsa, C. *Combust. Flame* **2011**, *158*, 227–239.
(53) El Bakali, A.; Mercier, X.; Wartel, M.; Acevedo, F.; Burns, I. S.; Gasnot, L.; Pauwels, J. F.; Desgroux, P. *Energy*, accepted for publication.
(54) Musick, M.; Van Tiggelen, P. J.; Vandooren, J. *Combust. Flame* **1996**, *105*, 433–450.

NOTE ADDED AFTER ASAP PUBLICATION

This article was published ASAP on November 9, 2011, with a text error in the second paragraph of the Experimental Setup section. The correct version was reposted on November 16, 2011.